coatings

MDPI

*Article*

# Study of the Photocatalytic Properties of Ni-Doped Nanotubular Titanium Oxide

**Fedor Zykov [1,2], Igor Selyanin [2], Roman Shishkin [2], Vadim Kartashov [1], Konstantin Borodianskiy [3,*] and Yuliy Yuferov [3,*]**

[1] Institute of Physics and Technology, Ural Federal University, 620002 Yekaterinburg, Russia
[2] Institute of Solid State Chemistry, Ural Branch of Russian Academy of Science, 620049 Yekaterinburg, Russia
[3] Department of Chemical Engineering, Ariel University, Ariel 40700, Israel
* Correspondence: konstantinb@ariel.ac.il (K.B.); yuliyy@ariel.ac.il (Y.Y.)

**Abstract:** Nanotubular titanium oxide is widely known as a prospective semiconductor photocatalyst for the process of water splitting. Its photoelectrochemical (PEC) efficiency can be improved by doping with 3d metal. In this work, the synthesis of nanotubular titanium oxide (NTO) was carried out by anodizing titanium substrates using two doping techniques. First, Ni-doped $TiO_2$ was obtained by immersion in Ni salt solution; second, an ethylene glycol-based fluoride electrolyte containing $Ni^{2+}$ ions solution was used. The obtained samples were analyzed using SEM, XRD, and photoelectrochemical methods. The produced Ni-doped NTO exhibited photocatalytic activity twice as high as that of nondoped NTO. Additionally, it was found that the immersion technique initiated a shift of the incident photon to converted electron (IPCE) spectra to the visible part of the spectrum.

**Keywords:** anodizing; IPCE; photoelectrochemistry; nanotubular titanium oxide



**Citation:** Zykov, F.; Selyanin, I.; Shishkin, R.; Kartashov, V.; Borodianskiy, K.; Yuferov, Y. Study of the Photocatalytic Properties of Ni-Doped Nanotubular Titanium Oxide. *Coatings* **2023**, *13*, 144. https://doi.org/10.3390/coatings13010144

Academic Editors: Dušan Galusek, Omid Sharifahmadian and Kamalan Kirubaharan Amirtharaj Mosas

Received: 19 December 2022
Revised: 4 January 2023
Accepted: 9 January 2023
Published: 11 January 2023



## 1. Introduction

In recent years, the progress of green hydrogen production has required obtaining more efficient materials for manufacturing. Among a high variety of such materials, titanium oxide is one of the most established. Titanium oxide is a photocatalyst that is used in solar energy harvesting in dye-sensitized solar cells and photocatalytic water splitting (PCWS). It is usually synthesized by the hydrolysis of titanium salt solutions [1,2], hydro or solvo-thermal techniques [3–6], chemical vapor deposition [7,8], and anodizing. The latter allows obtaining nanostructured oxide coatings with a large specific surface area on titanium [9–18], aluminum [19–26], and other metals and alloys [27–29]. Yuferov et al. previously studied the dependence of the photocatalytic properties of nanotubular titanium oxide (NTO) on the anodizing process [11]. Authors have shown that the change in anodizing parameters affects the photocatalytic properties; however, it has limitations in improving the photoelectrochemical (PEC) efficiency in PCWS processes. The usual main limitations are low tuning range of the conversion or optical bandgap, and low ability to affect to electron–hole recombination rate. Thus, research on the increase in PEC efficiency is required for applications in PCWS in the near future.

One of the most promising approaches in these regards is titania doping with metals of the 3d group. According to [30–34], doping $TiO_2$ with nickel can increase light absorption by including defect energy levels of the Ni 3d and narrowing its bandgap [33,35]. In [30], the authors proposed an adsorption mechanism of Ni onto anatase ($TiO_2$) by physisorption on five-fold coordinated Ti and chemisorption on surface hole sites. Only a few articles have been devoted to studying the photocatalytic properties of NTO decorated with nickel oxide [36] or metallic nickel [10,12,13,37–39]. In such instances, some progress was achieved in methylene blue photodegradation. It was detected that even small amounts of $Ni_xO_y$ or Ni particles in NTO can be beneficial; however, there are no data considering PCWS processes yet. Additionally, these particles form a heterojunction semiconductor

in the *p-n* scheme [13], which may enhance the utilization of the photogenerated holes with simultaneous photogeneration of electrons. However, they can shift to a lower energy level in the conduction and valence bands with subsequent recombination [17,37]. Nevertheless, even more complex modification techniques of double decoration have been studied. For example, sufficiently improved photocatalytic properties have been achieved by the decoration of NTO by the powder of Ni/Cr or NiS particles, which were used in previous works [3,16]. The outstanding photocatalytic properties of Ni-doped $TiO_2$ were also presented in [29,31]. However, these properties have been obtained using an expensive method of Ti-Ni alloy production.

This work presents a consideration of two cost-effective techniques for NTO doping by Ni. The first is the immersion of the NTO in a nickel salt solution, while the second is anodizing with $Ni(NO_3)_2$. A comparison of two doping approaches and the advantages of each are discussed in this work. Moreover, this work focuses on improving the PEC efficiency by the doping process in contrast to traditional Ni or NiO decoration methods.

## 2. Materials and Methods

Titanium metal (99.99%, VSMPO-AVISMA Corp., Verkhnyaya Salda, Russia) substrates for growing NTO were prepared by electrochemical polishing in a solution of ethylene glycol (99.9%, Ekos, Russia), 2-propanol (99.8 wt.%, Ekos, Russia) taken in volume ratios of 4:1, and NaCl 1 M (99.9%, Chemreactivsnab, Russia), by the method described earlier in [14,40,41]. Polishing was carried out at room temperature, maintaining a direct current voltage of 20 V for 50 min. Polished titania substrates were used for nanotube growth by anodizing in ethylene glycol with the addition of water and ammonium fluoride (99.9%, 40% water solution, Sigma-Tek, Russia) in volume ratios of 2.3% vol. and 1.5% mol, respectively. The synthesis of NTO was carried out for 40 min at a constant voltage of 30 V using an AKIP 1105 current source (Prist, Russia). The temperature of the electrolyte was set at 20 ± 1 °C. In the first method of doping, dried samples of amorphous NTOs were immersed in an aqueous solution of 0.05 or 0.1 M $Ni(NO_3)_2$ (99.9%, Chemreactivsnab, Russia) and kept for 0.5, 1, 2, and 3 h. They are named ID-x/y-NTO, where ID is immersion doped, x is the concentration of Ni salt, and y is the immersion time. Non-doped samples are named N-NTO. In the second one, Ni-doped $TiO_2$ samples were obtained by anodizing in the previously mentioned electrolyte with an addition of 0.05 or 0.1 M $Ni(NO_3)_2$, which are named AD-0.05-NTO and AD-0.10-NTO, respectively, where AD is anodized. Finally, all samples were heat-treated at a temperature of 400 °C in air, with a heating and cooling rate of 1 °C/min for the transition of amorphous nanotubular $TiO_2$ to the crystalline anatase phase.

Then, the phase compositions of the obtained coatings were determined by X-ray phase analysis (XRD) at room temperature using a STADI (STOE & Cie GmbH, Darmstadt Germany) diffractometer equipped with a CuKα X-ray source. Le-Bail analysis was carried out using Full Prof Suit software. The nanomorphology and chemical composition of the obtained NTOs were examined by scanning electron microscopy (SEM, Jeol JSM-6390LA, Jeol, Tokyo, Japan).

The PEC properties were measured using incident photon to converted electron spectroscopy (IPCE). SCS10-PEC (Zolix Instruments Co. Beijing, China) equipped with an electrochemical analyzer CHI600e was used to irradiate light at a given wavelength in the range from 300 to 480 nm with a step of 2.5 nm. IPCE measurements were conducted using a three-electrode cell with the following: the working electrode (WE)—NTO samples in the form of $Ti/TiO_2$ or $Ti/Ni\text{-}TiO_2$ plates, counter electrode (CE)—Pt, and the reference electrode (RE—Ag/AgCl and 0.1 M $KNO_3$ at an applied potential of 800 mV vs RE in accordance with procedures described elsewhere [11,15,42–44]. PEC activity was calculated according to the IPCE parameter by the following Equation (1):

$$IPCE = 1240 \cdot (Ip(\lambda))/(P(\lambda) \cdot \lambda), \quad (1)$$

where Ip(λ) is the photocurrent density at a given wavelength ($A \cdot m^{-2}$), P(λ) is the power of the light flux at a given wavelength ($W \cdot m^{-2}$), and λ is the incident light wavelength (nm). To examine the PEC properties based on current parameter measurements of the electrolyte cell during irradiation with light of a given wavelength at a given potential, the method is similar to that described in [11,44].

## 3. Results and Discussion

### *3.1. Coating Growth, Morphology and Chemical Composition*

Evaluation of the anodized NTO surface morphology revealed that the initial NTO microstructure was preserved within Ni doping approaches without considerable changes, as can be observed in the SEM image in Figure 1. This confirms that amorphous NTO neither dissolved nor degraded in nickel nitrate solution.

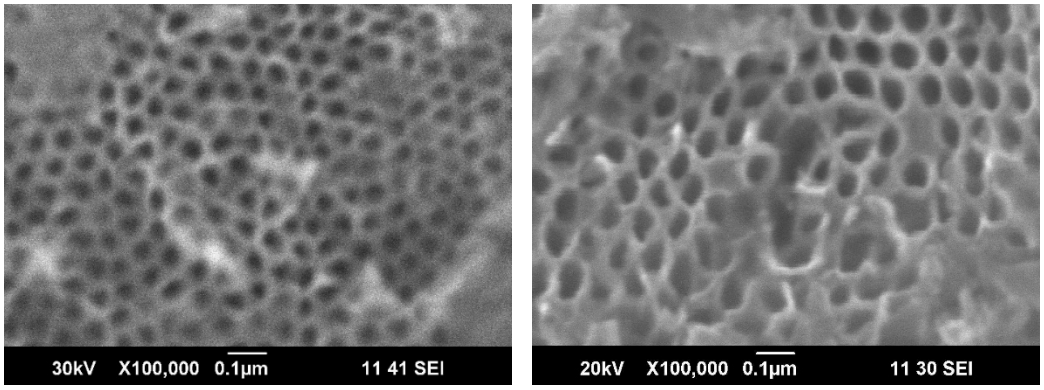


(**a**) (**b**)

**Figure 1.** Scanning electron microscopy (SEM) images of (**a**) ID-0.1/1-NTO and (**b**) AD-0.10-NTO.

The results of EDS analysis showed that the quantity of Ni in the samples did not exceed 3 at.%. The composition of the samples was calculated only by titanium and nickel elements. The concentration detection limit of Ni was approximately 1 at.%. The gathered data are presented in Table 1. It is clearly seen that $TiO_2$ doped by immersion contains significantly more Ni. Undetectable Ni in the anodized sample may be associated with a better distribution of Ni over the bulk and low penetration of the EDX signal.

**Table 1.** Composition of the samples studied in the work.

| Sample Name | Ni, at.% | Sample Name | Ni, at.% |
|---|---|---|---|
| N-NTO | 0 | N-NTO | 0 |
| ID-0.05/0.5-NTO | 0.8 | ID-0.10/0.5-NTO | 2.7 |
| ID-0.05/1-NTO | 1.9 | ID-0.10/1-NTO | 1.8 |
| ID-0.05/2-NTO | 1.5 | ID-0.10/2-NTO | 1.6 |
| ID-0.05/3-NTO | 1.0 | ID-0.10/3-NTO | 2.2 |
| AD-0.05-NTO | 0.0 | AD-0.10-NTO | 0.0 |

The SEM analysis of Ni-NTO did not reveal the exact structure of Ni compounds in NTO arrays in samples obtained by both doping methods. However, the detection of Ni may be due to its appearance on the NTO surface as a thin film or intergrain compound. Moreover, it should be noted that an increase in immersion time does not proportionally increase the amount of detected nickel in the NTO array.

### *3.2. Phase Analysis*

XRD patterns of the Ni-NTO samples annealed in air are shown in Figure 2a,b. The major phase formed during crystallization is anatase (A) with *I41/amd* symmetry. Some traces of unrecognized phases were observed in the patterns, which may be associated with

intermediate titanium oxide phases. The detected peaks are also confirmed by previous observations in [11]; however, due to the insufficient number of peaks, determination of phases is not possible. These phases may be attributed to a magneli-like type and are spontaneously formed and decompose from highly oriented titanium oxides. It was also detected that unrecognized titanium oxide phases disappear after a few weeks. The main diffraction peaks corresponding to crystal planes (100), (002), (101), (102), (110), and (103) are assigned to the titanium substrate (COD 96-901-6191). Anatase crystal planes (101), (103), (004), (200), (105), and (116) were detected (COD 96-901-5930) for samples doped by a concentration of nickel salt 0.05 and 0.10 M.

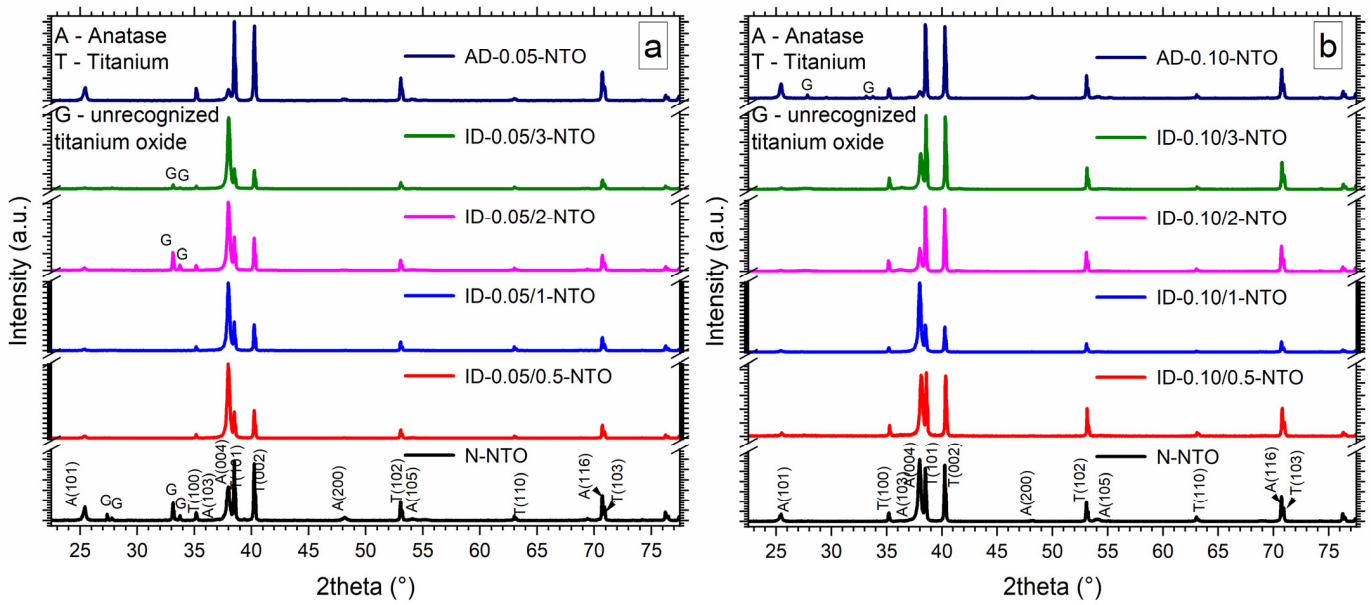


**Figure 2.** X-ray diffraction (XRD) patterns of nickel-doped nanostructured titanium oxide coatings obtained by anodizing for 40 min at 30 V for the sets of samples (**a**) N-NTO, ID-0.05/y-NTO, AD-0.05-NTO, and (**b**) N-NTO, ID-0.10/y-NTO, AD-0.10-NTO.

Interestingly, differences in the intensities of the (101) and (004) planes are clearly observed for different anodizing approaches. Samples ID-x/y-NTO display highly preferred oriented anatase on the (004) plane. Conversely, the AD-0.05-NTO and AD-0.10-NTO samples show a lower preferred orientation degree by the (004) plane. Hence, the Ni salt concentration in the last case does not sufficiently affect the phase composition of Ni-NTO (Figure 2) or the preferential orientation. This difference can be described as follows: in the first method, Ni ions from the nitrate solution are deposited on the surface of the NTO array and can react with amorphous titania during crystallization as illustrated in Figure 3a. In the second method, $Ni^{2+}$ ions present in electrolyte during anodizing can be directly introduced into the titania structure during anodic oxidation of the substrate as illustrated in Figure 3b. Such different paths of nickel doping result in preferred crystallization along different crystallographic axes.

Conversely, a higher $Ni^{2+}$ content in the electrolyte in the immersion approach forces the preferred orientation degree of anatase, which was recently considered in papers [11,45,46]. The disappearance of the (101) plane could be associated with a blocking effect due to the absorption of Ni onto the surface between the (101) planes, which was also considered in [47]. Here, $Ni^{2+}$ intercalates $TiO_2$ grains and after heat treatment, the position of Ni atoms can be considered interstitial. Moreover, the direct chemical reaction within pyrolysis of the NiO deposited particles could occur at a lower temperature than specified in [48], as a consequence of the higher activity of nanosized grains of NTO:

$$TiO_2 + NiO = NiTiO_3, \Delta G^{673K} = -15.601 \text{ kJ/mol}, \quad (2)$$

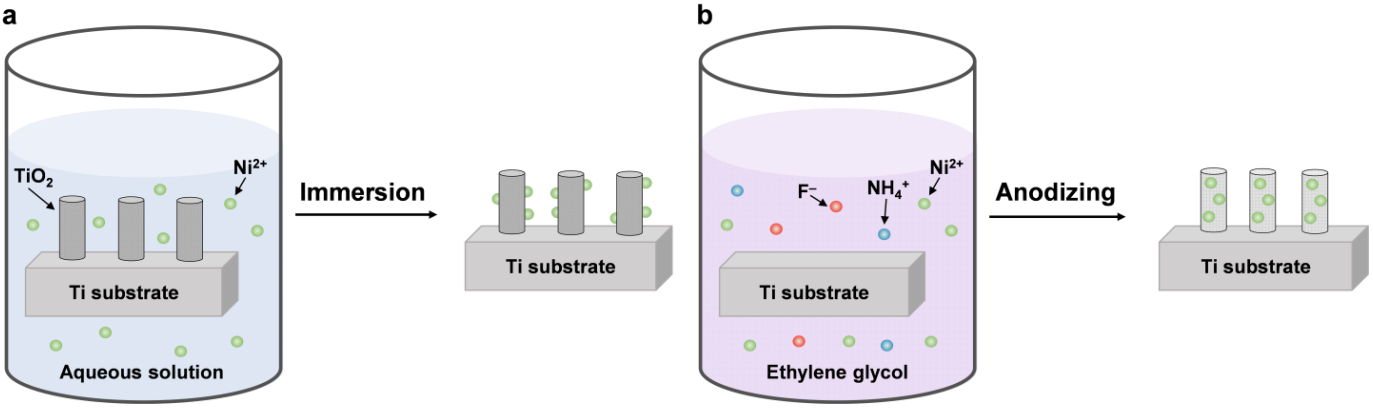


**Figure 3.** Schematics of Ni-doped $TiO_2$ formation by (**a**) immersion in an aqueous solution and (**b**) anodizing ethylene glycol.

The calculation of lattice parameters by the Le-Baile method for all the samples showed negligible variation. Pretty high nickel concentration investigated by EDX in the immersion series should give a noticeable change in case of solid solution of $Ti_{1-x}Ni_xO_{2-y}$ formation. As the lattice parameters remain unchanged, nickel is present at the surface of the NTO. The low nickel content in the AD-0.05-NTO and AD-0.10-NTO samples does not allow us to achieve an appreciable change in crystal lattice parameters, and the nickel distribution could not be directly confirmed by XRD measurements. However, because the initial orientation of NTO is retained during anodizing in Ni-containing electrolyte and the atomic radii of Ni and Ti atoms are close, it can be considered that a substitution solid solution is formed. Here, $Ti^{4+}$ atoms in $TiO_2$ can be substituted by $Ni^{2+}$ atoms, which enables additional energy defect levels in the energy level structure of the semiconductor.

On the one hand, the Ni doping approach significantly influences the preferred grain orientation, which could have completely different effects on the photocatalytic properties. On the other hand, the approaches used fail to achieve a sufficient concentration of Ni in NTO, which can be detected by the presence of any Ni-containing phases by XRD. This may be explained by their low content, thin film condition, amorphous state, or incorporation on Ti sites.

### *3.3. Photoelectrochemical Properties*

The results of the IPCE spectroscopy of the Ni-doped NTO samples are shown in Figure 4a,b. The similar results of the initial undoped NTO samples in both series show a high level of convergence of the measured results. The IPCE of the N-NTO sample peak position is approximately 355 ± 5 nm, and the maximum conversion in the peak position is 18 ± 1%. Figure 4a shows that N-NTO and AD-0.05-NTO have significant PEC efficiency. AD-0.05-NTO is referred to as mentioned earlier with the substitution of $Ti^{4+}$ by $Ni^{2+}$. The nonequal charge of particles results in enhanced oxygen non-stoichiometry for its compensation ($Ti_{1-x}Ni_xO_{2-y}$). A high concentration of charge carriers enables an increase in the peak intensity of the IPCE. However, sample ID-0.05/y-NTO has extremely low IPCE activity, less than 2% in the IPCE peak position. Such a phenomenon could be attributed to a chemical reaction of NiO particles with $TiO_2$, as shown in Equation (2). The produced $NiTiO_3$ (with a bandgap of 3.0 eV [49]) or surface thin film of nickel oxide forms a semiconductor heterostructure with $TiO_2$, which dramatically affects the IPCE efficiency. Unfortunately, this heterostructure decreases the PEC reaction efficiency by charge energy relaxation with subsequent recombination of the electron–hole pair, which has been widely considered elsewhere [50,51].

The same behavior is observed for ID-0.10/y-NTO (Figure 4b). It was observed that the increase in immersion time results in a crucial decrease in PEC activity. This behavior confirms the presence of deposited nickel oxide particles on the surface of anodized tita-

nium, followed by the formation of an insulating layer of $NiTiO_3$ during calcination. It is also obvious that a result is more pronounced for higher Ni salt concentrations because the content of these compounds increases.

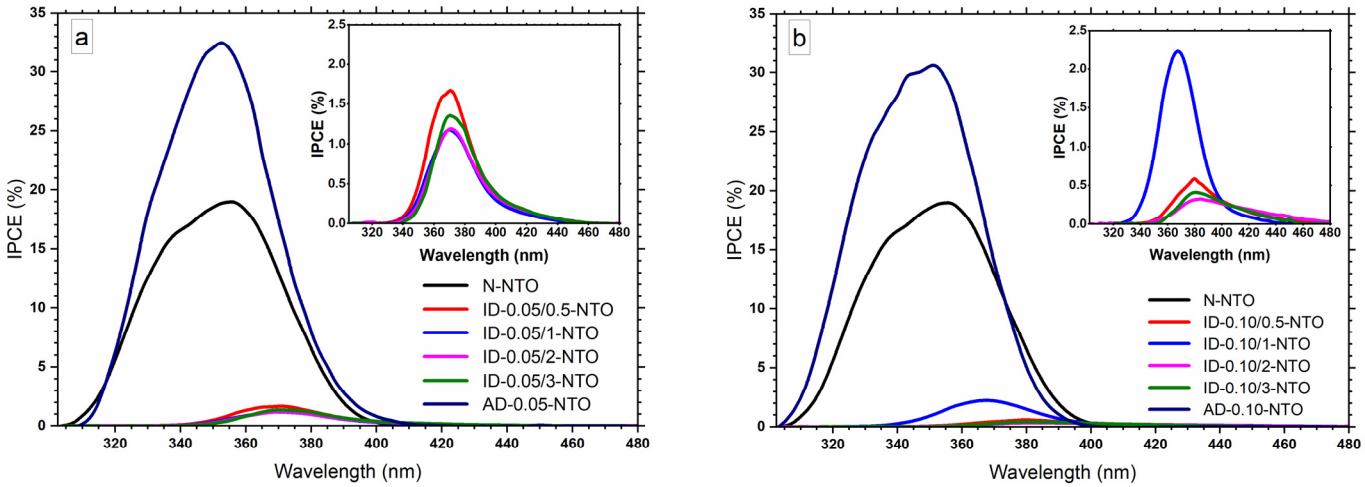


**Figure 4.** Incident photon to converted electron spectra (IPCE) of set of samples (**a**) N-NTO, ID-0.05/y-NTO, AD-0.05-NTO, and (**b**) N-NTO, ID-0.10/y-NTO, AD-0.10-NTO.

The set of ID-x/y-NTO samples exhibited low photocatalytic efficiency. The shift of the IPCE peak from 355 ± 5 to 380 ± 5 nm was caused by the formation of a heterojunction structure of $Ni_xO_y$ or $NiTiO_3$ with $TiO_2$, which formed by chemical reaction with a subtraction of decomposed $Ni(NO_3)_2$ on the NTO surface. Both the increase in recombination rate and lower value of $NiTiO_3$ band gap or $Ni_xO_y$ on the NTO surface negatively affect photocatalytic properties [52–54]. Simultaneously, interstitial Ni atoms were produced during anodizing with the initiation of an additional type of energy defect level. The conversion bandgap ($E_{ipce}$) and integer IPCE were calculated by the technique described elsewhere [11] and are presented in Table 2.

**Table 2.** Calculated conversion bandgap and integer IPCE of Ni-doped NTO.

| Sample Name | $E_{ipce}$, eV | Integer IPCE, % | Sample Name | $E_{ipce}$, eV | Integer IPCE, % |
|---|---|---|---|---|---|
| N-NTO | 3.26 ± 0.01 | 5.9 | N-NTO | 3.28 ± 0.01 | 4.2 |
| ID-0.05/0.5-NTO | 3.17 ± 0.01 | 0.4 | ID-0.10/0.5-NTO | 3.07 ± 0.02 | 0.2 |
| ID-0.05/1-NTO | 3.15 ± 0.01 | 0.3 | ID-0.10/1-NTO | 3.18 ± 0.01 | 0.5 |
| ID-0.05/2-NTO | 3.15 ± 0.01 | 0.3 | ID-0.10/2-NTO | 2.91 ± 0.02 | 0.1 |
| ID-0.05/3-NTO | 3.15 ± 0.02 | 0.3 | ID-0.10/3-NTO | 2.99 ± 0.01 | 0.1 |
| AD-0.05-NTO | 3.30 ± 0.02 | 8.8 | AD-0.10-NTO | 3.32 ± 0.02 | 8.9 |

It is clearly detected that anodizing with the $Ni(NO_3)_2$ additive positively affects the integral characteristics of Ni-doped NTO. Namely, the integer IPCE value increased more than twice. The IPCE peak position was not shifted, although its intensity increased more than 1.5 times. The advantageous IPCE can be attributed to the introduction of defect energy levels into the conduction and valence bands, which act as donors of the charge carriers. These levels improve the separation of photogenerated electron–hole pairs and positively affect the IPCE efficiency and PCWS processes. Thus, doping by anodizing with $Ni(NO_3)_2$ is more beneficial, which makes it possible to effectively consume the UV part of solar energy for the PCWS process. However, $E_{ipce}$ only of the immersed series decreased significantly from 3.28 to 2.91 and 3.26 to 3.15 eV for the ID-0.05/y-NTO and ID-0.10/y-NTO series, respectively.

## 4. Conclusions

Finally, anodizing with a doping additive is more effective than doping using the immersion technique. During the immersion technique, an inefficient heterojunction structure between titanium and nickel oxides is probably formed. This form increases the recombination rate of the photogenerated electron–hole pair. Although the peak position shifts to the visible part of the spectrum, the IPCE peak reaches less than 15% of the value of non-doped NTO. Simultaneously, anodizing with doping additives increases the IPCE peak by up to 1.5 times and the integral IPCE by more than two times. This behavior may be associated with $Ti^{4+}$ by $Ni^{2+}$ substitution with beneficial changes in the energy level structure of the semiconductor. It should be noted that immersion suppresses the crystallization of titania in the (101) plane, and the obtained material is extremely oriented by the (004) plane. This structure is formed due to the adsorption and formation of Ni-containing oxides onto the surface of $TiO_2$ arrays. Ni-doped titania obtained by anodizing has a traditional grain orientation of anatase. Here, the Ni atoms probably substituted the Ti atoms in the $TiO_2$ structure, which did not prevent the growth of grains in any direction.

The results of this research are relevant for the development of nanostructured semiconductor photoanodes based on titania for application in the PCWS process, providing additional input into the field of doping nanomaterials.

**Author Contributions:** Conceptualization, Y.Y., F.Z. and R.S.; methodology, Y.Y. and F.Z.; validation, Y.Y., F.Z. and R.S.; formal analysis, Y.Y., F.Z. and R.S.; investigation, F.Z., Y.Y., R.S. and I.S.; resources, Y.Y., F.Z., R.S., K.B., V.K. and I.S.; data curation, F.Z., Y.Y. and R.S.; writing—original draft preparation, Y.Y., F.Z., R.S. and K.B.; writing—review and editing, Y.Y., F.Z., R.S., I.S. and K.B.; visualization, Y.Y., F.Z. and R.S.; supervision, Y.Y., V.K. and K.B.; project administration, Y.Y. and V.K. All authors have read and agreed to the published version of the manuscript.

**Funding:** This research received no external funding.

**Institutional Review Board Statement:** Not applicable.

**Informed Consent Statement:** Not applicable.

**Data Availability Statement:** Not applicable.

**Acknowledgments:** The authors appreciate the support of this work within the government assignment № AAAA-A19-119110190048-7.

**Conflicts of Interest:** The authors declare no conflict of interest.

## References

1. Kay, A.; Grätzel, M. Low Cost Photovoltaic Modules Based on Dye Sensitized Nanocrystalline Titanium Dioxide and Carbon Powder. *Sol. Energy Mater. Sol. Cells* **1996**, *44*, 99–117. [CrossRef]
2. Zhang, J.; Huang, G.-F.; Li, D.; Zhou, B.-X.; Chang, S.; Pan, A.; Huang, W.-Q. Facile Route to Fabricate Carbon-Doped $TiO_2$ Nanoparticles and Its Mechanism of Enhanced Visible Light Photocatalytic Activity. *Appl. Phys. A* **2016**, *122*, 994. [CrossRef]
3. Shaban, M.; Ahmed, A.M.; Shehata, N.; Betiha, M.A.; Rabie, A.M. Ni-Doped and Ni/Cr Co-Doped $TiO_2$ Nanotubes for Enhancement of Photocatalytic Degradation of Methylene Blue. *J. Colloid. Interface Sci.* **2019**, *555*, 31–41. [CrossRef]
4. Gao, X.; Zhou, B.; Yuan, R. Doping a Metal (Ag, Al, Mn, Ni and Zn) on $TiO_2$ Nanotubes and Its Effect on Rhodamine B Photocatalytic Oxidation. *Environ. Eng. Res.* **2015**, *20*, 329–335. [CrossRef]
5. Vranješ, M.; Konstantinović, Z.; Pomar, A.; Kuljanin Jakovljević, J.; Stoiljković, M.; Nedeljković, J.M.; Šaponjić, Z. Room-Temperature Ferromagnetism in $Ni^{2+}$ Doped $TiO_2$ Nanocrystals Synthesized from Nanotubular Precursors. *J. Alloys Compd.* **2014**, *589*, 42–47. [CrossRef]
6. Lu, C.; Guan, W.; Hoang, T.K.A.; Guo, J.; Gou, H.; Yao, Y. Visible-Light-Driven Catalytic Degradation of Ciprofloxacin on Metal (Fe, Co, Ni) Doped Titanate Nanotubes Synthesized by One-Pot Approach. *J. Mater. Sci. Mater. Electron.* **2016**, *27*, 1966–1973. [CrossRef]
7. Shinde, P.S.; Bhosale, C.H. Properties of Chemical Vapour Deposited Nanocrystalline $TiO_2$ Thin Films and Their Use in Dye-Sensitized Solar Cells. *J. Anal. Appl. Pyrolysis* **2008**, *82*, 83–88. [CrossRef]
8. Alotaibi, A.M.; Sathasivam, S.; Williamson, B.A.D.; Kafizas, A.; Sotelo-Vazquez, C.; Taylor, A.; Scanlon, D.O.; Parkin, I.P. Chemical Vapor Deposition of Photocatalytically Active Pure Brookite $TiO_2$ Thin Films. *Chem. Mater.* **2018**, *30*, 1353–1361. [CrossRef]
9. Grimes, C.A.; Mor, G.K. *$TiO_2$ Nanotube Arrays*; Springer: Boston, MA, USA, 2009; ISBN 978-1-4419-0067-8.

10. Zhang, Y.; Yang, Y.; Xiao, P.; Zhang, X.; Lu, L.; Li, L. Preparation of Ni Nanoparticle-$TiO_2$ Nanotube Composite by Pulse Electrodeposition. *Mater. Lett.* **2009**, *63*, 2429–2431. [CrossRef]
11. Yuferov, Y.V.; Popov, I.D.; Zykov, F.M.; Suntsov, A.Y.; Baklanova, I.V.; Chukin, A.V.; Kukharenko, A.I.; Cholakh, S.O.; Zhidkov, I.S. Study of the Influence of Anodizing Parameters on the Photocatalytic Activity of Preferred Oriented $TiO_2$ Nanotubes Self-Doped by Carbon. *Appl. Surf. Sci.* **2022**, *573*, 151366. [CrossRef]
12. You, S.-M.; El Rouby, W.M.A.; Thamilselvan, A.; Tsai, C.-K.; Darmanto, W.; Doong, R.-A.; Millet, P. Fe/Ni Bimetallic Organic Framework Deposited on $TiO_2$ Nanotube Array for Enhancing Higher and Stable Photoelectrochemical Activity of Oxygen Evaluation Reaction. *Nanomaterials* **2020**, *10*, 1688. [CrossRef] [PubMed]
13. Díaz-Real, J.A.; Ortiz-Ortega, E.; Gurrola, M.P.; Ledesma-Garcia, J.; Arriaga, L.G. Light-Harvesting Ni/$TiO_2$ Nanotubes as Photo-Electrocatalyst for Alcohol Oxidation in Alkaline Media. *Electrochim. Acta* **2016**, *206*, 388–399. [CrossRef]
14. Zykov, F.; Yuferov, Y.; Kartashov, V. Photocatalytic Activity Boron-Doped $TiO_2$ Nanotubes. *AIP Conf. Proc.* **2022**, *2466*, 060017.
15. Kapusta-Kołodziej, J.; Chudecka, A.; Sulka, G.D. 3D Nanoporous Titania Formed by Anodization as a Promising Photoelectrode Material. *J. Electroanal. Chem.* **2018**, *823*, 221–233. [CrossRef]
16. Mollavali, M.; Falamaki, C.; Rohani, S. High Performance NiS-Nanoparticles Sensitized $TiO_2$ Nanotube Arrays for Water Reduction. *Int. J. Hydrog. Energy* **2016**, *41*, 5887–5901. [CrossRef]
17. Li, H.; Zhou, J.; Zhang, X.; Zhou, K.; Qu, S.; Wang, J.; Lu, X.; Weng, J.; Feng, B. Constructing Stable NiO/N-Doped $TiO_2$ Nanotubes Photocatalyst with Enhanced Visible-Light Photocatalytic Activity. *J. Mater. Sci. Mater. Electron.* **2015**, *26*, 2571–2578. [CrossRef]
18. Etacheri, V.; Di Valentin, C.; Schneider, J.; Bahnemann, D.; Pillai, S.C. Visible-Light Activation of $TiO_2$ Photocatalysts: Advances in Theory and Experiments. *J. Photochem. Photobiol. C Photochem. Rev.* **2015**, *25*, 1–29. [CrossRef]
19. Sulka, G.D. Highly Ordered Anodic Porous Alumina Formation by Self-Organized Anodizing. In *Nanostructured Materials in Electrochemistry*; Wiley-VCH Verlag GmbH & Co. KGaA: Weinheim, Germany, 2008; pp. 1–116. ISBN 9783527318766.
20. Yuferov, Y.V.; Zykov, F.M.; Malshakova, E. Defects of Porous Self-Structured Anodic Alumina Oxide on Industrial Aluminum Grades. *Solid State Phenom.* **2018**, *284*, 1134–1139. [CrossRef]
21. Leontiev, A.P.; Roslyakov, I.V.; Napolskii, K.S. Complex Influence of Temperature on Oxalic Acid Anodizing of Aluminium. *Electrochim. Acta* **2019**, *319*, 88–94. [CrossRef]
22. Yuferov, Y.V.; Arnautov, A.I.; Chukin, A.V.; Schak, A.V.; Shishkin, R.A. Development of a Technology for Obtaining a Multilayer Nanoporous Aluminium Oxide. *AIP Conf. Proc.* **2019**, *2174*, 020188.
23. Popov, N.; Vasin, A.; Yuferov, Y.; Popov, I. Luminescence of Nanoporous Anodic Oxide Obtained from Rare Earth Doped Aluminum. *AIP Conf. Proc.* **2019**, *2174*, 020051.
24. Arnautov, A.; Yuferov, Y.; Zykov, F.; Chukin, A.; Kudyakova, V.; Shishkin, R. Improvement of the Electro Insulating Characteristics of Anodic Nanoporous Aluminum Oxide Insulator by Filling with Silicon Dioxide. *AIP Conf. Proc.* **2019**, *2174*, 020004.
25. Pashchanka, M. Conceptual Progress for Explaining and Predicting Self-Organization on Anodized Aluminum Surfaces. *Nanomaterials* **2021**, *11*, 2271. [CrossRef]
26. Yuferov, Y.; Arnautov, A.; Shak, A.; Beketov, A. Forming Complex Geometry of Nanopore by Anodic Oxidation of Aluminum by Pulsation Method. *AIP Conf. Proc.* **2018**, *2015*, 020113.
27. Yang, M.; Huo, L.; Pei, L.; Pan, K.; Gan, Y. Enhanced Photoelectrochemical Performance and Charge Transfer Properties in Self-Organized NiOx-Doped $TiO_2$ Nanotubes. *Electrochim. Acta* **2014**, *125*, 288–293. [CrossRef]
28. Wang, H.; Jin, K.; Dong, X.; Zhan, S.; Liu, C. Preparation Technique and Properties of Nano-$TiO_2$ Photocatalytic Coatings for Asphalt Pavement. *Appl. Sci.* **2018**, *8*, 2049. [CrossRef]
29. Liu, Q.; Ding, D.; Ning, C.; Wang, X. Black Ni-Doped $TiO_2$ Photoanodes for High-Efficiency Photoelectrochemical Water-Splitting. *Int. J. Hydrog. Energy* **2015**, *40*, 2107–2114. [CrossRef]
30. Escamilla-Roa, E.; Timón, V.; Hernández-Laguna, A. DFT Study of the Adsorption of Ni on Anatase (001) Surface. *Comput. Theor. Chem.* **2012**, *981*, 59–67. [CrossRef]
31. Dong, Z.; Ding, D.; Li, T.; Ning, C. Ni-Doped $TiO_2$ Nanotubes Photoanode for Enhanced Photoelectrochemical Water Splitting. *Appl. Surf. Sci.* **2018**, *443*, 321–328. [CrossRef]
32. Wang, Y.; Zhang, R.; Li, J.; Li, L.; Lin, S. First-Principles Study on Transition Metal-Doped Anatase $TiO_2$. *Nanoscale Res. Lett.* **2014**, *9*, 46. [CrossRef] [PubMed]
33. D'yachkov, E.P.; Makaev, D.V.; Khoroshavin, L.O.; D'yachkov, P.N. Effect of 3d-Metal Dopants on the Electronic Properties of Hexagonal Titanium Dioxide Nanotubes. *Russ. J. Inorg. Chem.* **2017**, *62*, 931–934. [CrossRef]
34. Lin, Y.; Jiang, Z.; Zhu, C.; Zhang, R.; Hu, X.; Zhang, X.; Zhu, H.; Lin, S.H. The Electronic Structure, Optical Absorption and Photocatalytic Water Splitting of (Fe + Ni)-Codoped $TiO_2$: A DFT +U Study. *Int. J. Hydrogen Energy* **2017**, *42*, 4966–4976. [CrossRef]
35. Yuan, R.; Zhou, B.; Hua, D.; Shi, C. Effect of Metal Ion-Doping on Characteristics and Photocatalytic Activity of $TiO_2$ Nanotubes for Removal of Humic Acid from Water. *Front. Environ. Sci. Eng.* **2015**, *9*, 850–860. [CrossRef]
36. Sim, L.C.; Ng, K.W.; Ibrahim, S.; Saravanan, P. Preparation of Improved P-n Junction NiO/$TiO_2$ Nanotubes for Solar-Energy-Driven Light Photocatalysis. *Int. J. Photoenergy* **2013**, *2013*, 659013. [CrossRef]
37. Cheshideh, H.; Nasirpouri, F. Cyclic Voltammetry Deposition of Nickel Nanoparticles on $TiO_2$ Nanotubes and Their Enhanced Properties for Electro-Oxidation of Methanol. *J. Electroanal. Chem.* **2017**, *797*, 121–133. [CrossRef]
38. Ren, K.; Gan, Y.X.; Young, T.J.; Moutassem, Z.M.; Zhang, L. Photoelectrochemical Responses of Doped and Coated Titanium Dioxide Composite Nanotube Anodes. *Compos. Part B Eng.* **2013**, *52*, 292–302. [CrossRef]

39. Liang, F.; Zhang, J.; Zheng, L.; Tsang, C.-K.; Li, H.; Shu, S.; Cheng, H.; Li, Y.Y. Selective Electrodeposition of Ni into the Intertubular Voids of Anodic TiO 2 Nanotubes for Improved Photocatalytic Properties. *J. Mater. Res.* **2013**, *28*, 405–410. [CrossRef]
40. Kim, D.; Son, K.; Sung, D.; Kim, Y.; Chung, W. Effect of Added Ethanol in Ethylene Glycol–NaCl Electrolyte on Titanium Electropolishing. *Corros. Sci.* **2015**, *98*, 494–499. [CrossRef]
41. Ferreri, N.C.; Savage, D.J.; Knezevic, M. Non-Acid, Alcohol-Based Electropolishing Enables High-Quality Electron Backscatter Diffraction Characterization of Titanium and Its Alloys: Application to Pure Ti and Ti-6Al-4V. *Mater. Charact.* **2020**, *166*, 110406. [CrossRef]
42. Kapusta-Kołodziej, J.; Syrek, K.; Sulka, G.D. Synthesis and Photoelectrochemical Properties of Anodic Oxide Films on Titanium Formed by Pulse Anodization. *J. Electrochem. Soc.* **2018**, *165*, H838–H844. [CrossRef]
43. Kapusta-Kołodziej, J.; Syrek, K.; Pawlik, A.; Jarosz, M.; Tynkevych, O.; Sulka, G.D. Effects of Anodizing Potential and Temperature on the Growth of Anodic $TiO_2$ and Its Photoelectrochemical Properties. *Appl. Surf. Sci.* **2017**, *396*, 1119–1129. [CrossRef]
44. Chen, Z.; Dinh, H.N.; Miller, E. *Photoelectrochemical Water Splitting*; SpringerBriefs in Energy; Springer: New York, NY, USA, 2013; ISBN 978-1-4614-8297-0.
45. Wang, L.; Wang, Y.; Yang, Y.; Wen, X.; Xiang, H.; Li, Y. Fabrication of Different Crystallographically Oriented $TiO_2$ Nanotube Arrays Used in Dye-Sensitized Solar Cells. *RSC Adv.* **2015**, *5*, 41120–41124. [CrossRef]
46. Einollahzadeh-Samadi, M.; Dariani, R.S.; Paul, A. Tailoring Morphology, Structure and Photoluminescence Properties of Anodic $TiO_2$ Nanotubes. *J. Appl. Crystallogr.* **2017**, *50*, 1133–1143. [CrossRef]
47. Treacy, J.P.W.; Hussain, H.; Torrelles, X.; Grinter, D.C.; Cabailh, G.; Bikondoa, O.; Nicklin, C.; Selcuk, S.; Selloni, A.; Lindsay, R.; et al. Geometric Structure of Anatase $TiO_2$ (101). *Phys. Rev. B* **2017**, *95*, 075416. [CrossRef]
48. Lin, Y.-J.; Chang, Y.-H.; Yang, W.-D.; Tsai, B.-S. Synthesis and Characterization of Ilmenite $NiTiO_3$ and $CoTiO_3$ Prepared by a Modified Pechini Method. *J. Non. Cryst. Solids* **2006**, *352*, 789–794. [CrossRef]
49. Li, M.-W.; Yuan, J.-P.; Gao, X.-M.; Liang, E.-Q.; Wang, C.-Y. Structure and Optical Absorption Properties of $NiTiO_3$ Nanocrystallites. *Appl. Phys. A* **2016**, *122*, 725. [CrossRef]
50. Xu, Q.; Zhang, L.; Yu, J.; Wageh, S.; Al-Ghamdi, A.A.; Jaroniec, M. Direct Z-Scheme Photocatalysts: Principles, Synthesis, and Applications. *Mater. Today* **2018**, *21*, 1042–1063. [CrossRef]
51. Hassani, A.; Krishnan, S.; Scaria, J.; Eghbali, P.; Nidheesh, P.V. Z-Scheme Photocatalysts for Visible-Light-Driven Pollutants Degradation: A Review on Recent Advancements. *Curr. Opin. Solid State Mater. Sci.* **2021**, *25*, 100941. [CrossRef]
52. Fan, X.; Zhang, Y.; Xiao, P.; Hu, F.; Zhang, H. Preparation of High-Orderly $TiO_2$ Nanotubes in Organic Solution and Characterization of C-Doped $TiO_2$. *Chinese J. Chem. Phys.* **2007**, *20*, 753–758. [CrossRef]
53. Malato, S.; Fernández-Ibáñez, P.; Maldonado, M.I.; Blanco, J.; Gernjak, W. Decontamination and Disinfection of Water by Solar Photocatalysis: Recent Overview and Trends. *Catal. Today* **2009**, *147*, 1–59. [CrossRef]
54. Liu, G.; Sun, C.; Cheng, L.; Jin, Y.; Lu, H.; Wang, L.; Smith, S.C.; Lu, G.Q.; Cheng, H. Efficient Promotion of Anatase $TiO_2$ Photocatalysis via Bifunctional Surface-Terminating Ti–O–B–N Structures. *J. Phys. Chem. C* **2009**, *113*, 12317–12324. [CrossRef]